J. Fluid Mech. (2013), *vol.* 732, *pp.* 5–28.
doi:10.1017/jfm.2013.382

The elastic Landau–Levich problem

Harish N. Dixit† **and G. M. Homsy**

Department of Mathematics, University of British Columbia, 1984 Mathematics Road, Vancouver, BC, V6T 1Z2, Canada

(Received 24 January 2013; revised 14 July 2013; accepted 20 July 2013; first published online 30 August 2013)

We study the classical Landau–Levich dip-coating problem in the case where the interface has significant elasticity. One aim of this work is to unravel the effect of surface-adsorbed hydrophobic particles on Landau–Levich flow. Motivated by recent findings (Vella, Aussillous & Mahadevan, *Europhys. Lett.*, vol. 68, 2004, pp. 212–218) that a jammed monolayer of adsorbed particles on a fluid interface makes it respond akin to an elastic solid, we use the Helfrich elasticity model to study the effect of interfacial elasticity on Landau–Levich flow. We define an elasticity number, El, which represents the relative strength of viscous forces to elasticity. The main assumptions of the theory are that El be small, and that surface tension effects are negligible. The shape of the free surface is formulated as a nonlinear boundary value problem: we develop the solution as an asymptotic expansion in the small parameter $El^{1/7}$ and use the method of matched asymptotic expansions to determine the film thickness as a function of El. The solution to the shape of the static meniscus is not as straightforward as in the classical Landau–Levich problem, as evaluation of higher-order effects is necessary in order to close the problem. A remarkable aspect of the problem is the occurrence of multiple solutions, and five of these are found numerically. In any event, the film thickness varies as $El^{4/7}$ in qualitative agreement with the experiments of Ouriemi & Homsy (*Phys. Fluids*, 2013, in press).

Key words: capillary flows, lubrication theory, coating

1. Introduction

One of the most fundamental fluid mechanical processes is the coating of a wall or a plate. In a laboratory setting, it is common to withdraw a submerged plate from a reservoir of fluid, thus coating the plate with a thin film of fluid. This is the classical Landau–Levich dip coating flow. If U is the speed of withdrawal of a vertical plate, μ is the viscosity of the fluid and σ is the surface tension of the fluid–gas interface, the problem is governed by the capillary number, $Ca = \mu U/\sigma$. Landau & Levich (1942) and Derjaguin (1943) theoretically obtained the classical Landau–Levich law which gives the coating thickness in the fully developed region, $\bar{h}_{\infty,c}$, as

$$\tilde{h}_{\infty,c} = 0.9458 l_c Ca^{2/3} \tag{1.1}$$

where $l_c = \sqrt{\sigma/\rho g}$ is the capillary length with ρ being the density of the underlying fluid and g being gravity. Closely related to the Landau–Levich flow is the so-called

† Email address for correspondence: hdixit@math.ubc.ca

Bretherton problem (Bretherton 1961) where a thin film is deposited on the inner walls of a tube when a low-viscosity fluid displaces a high-viscosity fluid. Other related problems are the coating of fibres (see Quéré 1999 and references therein), roll-coating on a tube (Gaskell *et al.* 1995) and film coating in a Hele-Shaw cell (Park & Homsy 1984).

The Landau–Levich problem for a clean, no tangential-stress interface has been verified experimentally on numerous occasions (see, for example, Groenveld 1970*a*; Krechetnikov & Homsy 2005 and references therein). Both the Landau–Levich and Bretherton problems have been a focus of intense study for the last four decades not only due to their fundamental importance, but also because of some puzzling results found in experiments. What began as a investigation into the apparent discrepancy between Bretherton's theoretical and experimental results for capillary numbers smaller than 10^{-4} has evolved into a separate study on the role of surface impurities in the coating process. Commonly encountered impurities are either surfactants or colloidal particles residing both in the bulk and on the interface. Surfactants lower the surface tension of the interface producing a Marangoni effect resulting in film thickening relative to that obtained with a clean interface. Groenveld (1970*b*) investigated the role of surface impurities and obtained a film thickness twice that of the clean case. Ratulowski & Chang (1990) and Stebe & Barthès-Biesel (1995) developed asymptotic analysis for the Bretherton problem and obtained film thickening whose upper bound was found to be a factor of $4^{2/3}$ over the clean interface case. Mayer & Krechetnikov (2012) found that Groenveld was the first to obtain this $4^{2/3}$ bound, which was reported incorrectly in his publication. Park (1991) developed an asymptotic theory for insoluble surfactants and found the same upper bound. Both Groenveld (1970*b*) and Park (1991) concluded that the interfacial stagnation point found in the clean case disappears. Upon extracting the flow field from Park's analysis, we found that the interfacial stagnation point becomes a saddle point in the bulk. This latter flow field was recently obtained using numerical simulations by Campana *et al.* (2010) for soluble surfactants and by Campana *et al.* (2011) in the case of insoluble surfactants. Mayer & Krechetnikov (2012) recently conducted a systematic flow visualization study using SDS surfactants and revealed the saddle-point structure of the flow field near the plate.

Coating flows with surfactants also has an important application in the formation of Langmuir–Blodgett films, but in these films the surfactant concentration is typically high, with the interface covered by a uniform monolayer of surfactants. Surfactant effects in the Bretherton problem have an important biological application: liquid occlusions in the lungs prevent airways from opening, resulting in respiratory distress syndrome in infants. It is believed that lack of surfactants prevent the airways from reopening, and much effort has been devoted to understanding this mechanism (see Gaver, Samsel & Solway 1990; Gaver *et al.* 1996; Jensen *et al.* 2002; Grotberg & Jensen 2004). However, unlike the classical Bretherton problem, the capillaries are flexible and the wall elasticity plays an important role in the fluid mechanical process. In the above studies, wall elasticity is treated using linear springs which are flexible in a direction perpendicular to the motion of the bubble. Finally, in addition to biological films such as lipid bilayers, amphiphilic films can be formed with surfactants. The well-known Helfrich elasticity model (Helfrich 1973), has been widely used to model elasticity in such surfactant films (Szleifer *et al.* 1990; Daicic *et al.* 1996; Würger 2000), although the origins of elastic constants in the model in this case are still an area of active research.

Particles at interfaces can also lead to important surface forces, and they have strong similarities with surfactants, as discussed in a review by Binks (2002). The role of particles in stabilizing emulsions is well known. Ramsden (1903) and Pickering (1907) first noticed how emulsions can be stabilized by using particles to coat the interface between the two phases. Kruglyakov & Nushtayeva (2004) give a modern account of the role of particles in stabilization of emulsions. Floating particles on an interface experience long-range capillary attraction forces (Nicolson 1949; Gifford & Scriven 1971; Chan, Henry & White 1981; Danov & Kralchevsky 2010). In the absence of any surface charge, these forces cause the particles to stick to each other, forming a monolayer on the interface. Such a monolayer can be used to shield drops and bubbles from the surrounding environment by forming 'armour' at the interface (Dinsmore *et al.* 2002; Subramaniam, Abkarian & Stone 2005*b*). This can be exploited to create hydrophobic liquid 'marbles' with fluid encapsulated by tiny colloidal hydrophobic particles (Aussillous & Quéré 2001; McHale & Newton 2011). In general, particle-laden interfaces exhibit three different states depending on the surface concentration of the particles (Monteux *et al.* 2007). At low concentrations when the particles are separated from each other, the interface is said to be in a fluid state and is dominated by surface tension. The interface exhibits solid-like characteristics when the particles get into a jammed state and if the particle concentration is further increased, the interface buckles. At the onset of buckling, Monteux *et al.* (2007) showed that the surface tension of the interface drops to zero. Within the jammed state, Varshney *et al.* (2012) showed a phase transition from a less-rigid state where the interface is a capillary bridged solid to a more-rigid state where the interface is a dominated by frictional contacts between the particles. Interfacial rheology of such systems has been studied by Reynaert, Moldenaers & Vermant (2007) and is also discussed in a recent review by Fuller & Vermant (2012).

The above works suggest that the presence of a monolayer of particles can drastically change the mechanical properties of the interface. Vella, Aussillous & Mahadevan (2004) show that a jammed monolayer of floating particles responds like an elastic sheet undergoing a buckling instability on compression. Using the wavelength of the instability, the authors calculate the Young's modulus of the particle raft assuming an elastic response for small interface deformations. The authors suggest that the interface deformation can be described by a beam equation

$$B\frac{\mathrm{d}^4h}{\mathrm{d}x^4} + T\frac{\mathrm{d}^2h}{\mathrm{d}x^2} + \rho gh = 0, \tag{1.2}$$

where B is the bending stiffness of the sheet, T is the compressive force per unit length in the sheet, g is gravity and $h(x)$ is the deformation of the interface from its equilibrium horizontal position. For large deformations to an interface, particles can undergo spatial rearrangements. In terms of an energy landscape, if the new configuration has a lower energy compared with the old configuration, then the system can undergo permanent plastic deformation. This was demonstrated by Subramaniam *et al.* (2005*a*) where a bubble covered with particles was shown to assume non-spherical shapes. Interestingly, Yunker *et al.* (2012) show that anisotropic particles can lead to increased bending rigidity of the interfaces.

There is also relevant literature on floating elastic sheets. Buckling and wrinkling of elastic films over a fluid/gel surface has been studied by many authors in recent years (see Pocivavsek *et al.* (2008) and Audoly (2011) and references therein). Remarkably, Diamant & Witten (2011) show that in two dimensions, the static interface shape can be obtained analytically. The interaction of an elastic membrane with a fluid interface

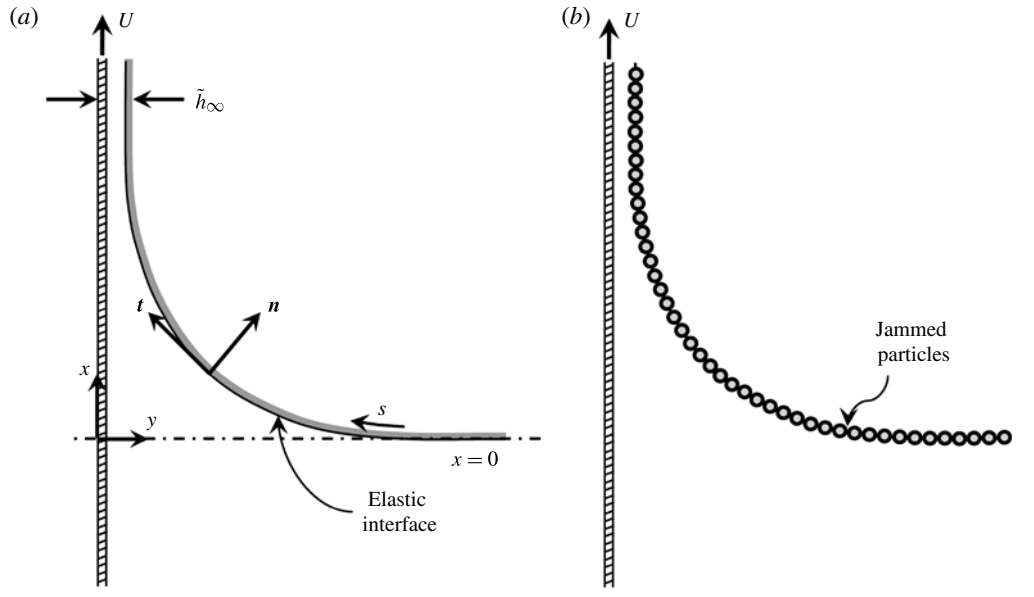

FIGURE 1. A schematic of the Landau–Levich dip-coating problem (*a*) with the interface represented as an elastic sheet and (*b*) with a jammed monolayer of particles. The Cartesian coordinates x and y are directed along the plate and on the undisturbed flat interface, respectively, and s is the arclength coordinate directed along the tangent vector.

can also lead to interesting elastocapillary problems such as capillary origami (Py *et al.* 2007), where an elastic sheet spontaneously wraps around a drop to create three-dimensional origami-type shapes.

These various phenomena involving surfactants at high concentration, particles adsorbed at interfaces, and elastic sheets at interfaces all raise the interesting question of the role of elasticity on the dip-coating process. In this paper, we theoretically examine the role of interfacial elasticity on the Landau–Levich flow, employing the well-known Helfrich elasticity model (Helfrich 1973), a model that is widely used to mimic elasticity in lipid bilayers. Figure 1(*a*) shows the basic model, the formulation of which is given in the next section.

The work considered in this paper was motivated in part by experiments by Ouriemi & Homsy (2013) who showed that surface-adsorbed hydrophobic particles can lead to film thickening in the Landau–Levich flow. Floating particles cause two primary changes to an interface: (i) they alter the surface tension of the interface (Okubo 1995; Fainerman *et al.* 2006); and (ii) they produce an elastic response as discussed above. The former effect is similar to that of surfactants and arises when the particle concentration changes along the interface. We focus on the second of these effects and assume that the particles form a monolayer that entirely covers the fluid interface and that the particles are always in a jammed state, as shown in figure 1(*b*). In such a scenario, the concentration of particles is fixed along the interface at the limiting concentration.

It is important to sound a word of caution in relating the idealized elastic model to a particle-laden interface in a coating flow. In reality, the concentration of particles may vary along the interface. This in turn will affect the flow field in the bulk as a result of variable surface tension and variable elasticity and the corresponding generalized

Marangoni effects. In addition, particle diffusion and adsorption/desorption could also be important. While not unaware of these possibilities, we restrict this study to the case of constant particle concentration (and, hence, to constant interfacial elasticity) as a necessary first step in building understanding of coating of a broad class of interfacial materials that exhibit elasticity. We hope that such a study will motivate further research into particle-laden interfaces. Indeed, as greater understanding of particle-laden interfaces is gained, the present theory can be extended to include the case of variable particle concentration. Finally, in the current paper, we neglect the role of surface tension assuming that elasticity affects dominate over surface tension effects. The combined effects of elasticity and surface tension will be analysed in a subsequent companion paper.

The paper is organized as follows. In § 2, we first introduce the governing equations in dimensional and non-dimensional forms with a discussion of various scalings and non-dimensional numbers. In § 3, the asymptotic analysis is presented for the leading order equations along with the relevant matching conditions. We then obtain the solution to a static elastic meniscus in § 4. In § 5, the solution to the elastic Landau–Levich (ELL) equation is obtained. Section 6 summarizes the paper, compares the present theory with experiments of Ouriemi & Homsy (2013) and discusses possible extensions and applications of the theory developed here.

2. Governing equations and scalings

Consider a vertical flat plate rising from a reservoir of fluid with a constant velocity, U, as shown schematically in figure 1(a). The density of the fluid is ρ and we neglect the effect of the surrounding air. The schematic shows the flat interface at $x = 0$ covered with a jammed monolayer of particles. We further assume that the particle size is much smaller than the film thickness in the fully developed region. The governing equations for the fluid below the interface in steady-state conditions can then be written in dimensional form as

$$\nabla \cdot \tilde{\boldsymbol{u}} = 0, \tag{2.1a}$$

$$\tilde{\boldsymbol{u}} \cdot \nabla \tilde{\boldsymbol{u}} = -\frac{1}{\rho}\nabla \tilde{p} + \frac{\mu}{\rho}\nabla^2 \tilde{\boldsymbol{u}} + \boldsymbol{g} \tag{2.1b}$$

where $\tilde{\boldsymbol{u}}$ is the dimensional velocity, ρ is the density of the fluid, $\boldsymbol{g}$ is the gravity, μ is the dynamic viscosity and $\tilde{p}$ is the dimensional pressure.

As discussed, the presence of particles at the interface modifies the stress boundary condition there. We model the particle-laden film using the Helfrich model (Helfrich 1973) for the elastic energy E_c,

$$E_C = \frac{1}{2}\int K_B(\tilde{\kappa} - \tilde{\kappa}_0)^2 \,\mathrm{d}A + \oint \gamma \,\mathrm{d}C, \tag{2.2}$$

where K_B is the bending modulus, and $\tilde{\kappa}$ and $\tilde{\kappa}_0$ are the dimensional mean and spontaneous curvatures, respectively. In the first term, the integration is performed over the surface area of the interface, and in the second term, the integration is performed around the particle-raft 'islands' representing the contribution from the line tension, γ. This term does not enter the present analysis since we assume that the particles are in a completely jammed state throughout the interface and the analysis is restricted to two dimensions. If the size of the particles is small in relation to the mean radius of curvature of the interface, it can be shown that spontaneous curvature is small (Planchette, Lorenceau & Biance 2012), and hence we neglect $\tilde{\kappa}_0$ in the present

analysis. In the absence of particles, there is an additional free energy contribution from surface tension,

$$E_T = \int \sigma \, \mathrm{d}A, \tag{2.3}$$

where σ is the surface tension of the interface. In the present paper, we neglect surface tension and assume that the interface shape is wholly described by a balance of viscous, gravitational and elastic effects.

For a two-dimensional interface, the integration is performed along a line, and hence dA can be replaced by ds, where s is the arclength coordinate measured in the direction of the tangent as shown in figure 1(a). Using the procedure given in Kaoui *et al.* (2008), we derive expressions for the interfacial forces from (2.2), which are given by

$$\boldsymbol{f}_c = -K_B \left(\frac{\partial^2 \tilde{\kappa}}{\partial s^2} + \frac{\tilde{\kappa}^3}{2} \right) \boldsymbol{n}, \tag{2.4}$$

where $\boldsymbol{n}$ is unit vector in the normal direction. In deriving (2.4), we assumed a constant modulus K_B. The normal and tangential stress balance equations on the interface at $y = h(x)$ then take the form

$$\boldsymbol{n} \cdot \tilde{\boldsymbol{T}} \cdot \boldsymbol{n} = -K_B \left(\frac{\partial^2 \tilde{\kappa}}{\partial s^2} + \frac{\tilde{\kappa}^3}{2} \right), \tag{2.5a}$$

$$\boldsymbol{t} \cdot \tilde{\boldsymbol{T}} \cdot \boldsymbol{n} = 0, \tag{2.5b}$$

where $\boldsymbol{t}$ is the unit vector in the tangential direction and $\tilde{\boldsymbol{T}} = -\tilde{p}\boldsymbol{I} + \mu[\boldsymbol{\nabla}\tilde{\boldsymbol{u}} + \boldsymbol{\nabla}\tilde{\boldsymbol{u}}^{\mathrm{T}}]$ is the stress tensor. In writing these equations, the effect of interfacial viscosity is neglected. The remaining boundary conditions on the plate and the free-surface are given by

$$\tilde{\boldsymbol{u}} = \tilde{\boldsymbol{U}} \quad \text{at } \tilde{y} = 0, \tag{2.6}$$

$$\boldsymbol{n} \cdot \tilde{\boldsymbol{u}} = 0 \quad \text{at } \tilde{y} = \tilde{h}(\tilde{x}). \tag{2.7}$$

Being dimensionless, the tilde decoration is not used for the normal and tangential vectors. In terms of free-surface shape, $\tilde{h}(\tilde{x})$, these vectors take the form

$$\boldsymbol{n} = \frac{-\tilde{h}_{\tilde{x}}\hat{i} + \hat{j}}{(1 + \tilde{h}_{\tilde{x}}^2)^{1/2}}, \quad \boldsymbol{t} = \frac{\hat{i} + \tilde{h}_{\tilde{x}}\hat{j}}{(1 + \tilde{h}_{\tilde{x}}^2)^{1/2}} \quad \text{with } \tilde{h}_{\tilde{x}} = \frac{\mathrm{d}\tilde{h}}{\mathrm{d}\tilde{x}}, \tag{2.8}$$

where $\hat{i}$ and $\hat{j}$ are the unit vectors in the x and y directions respectively. The dimensional curvature, $\tilde{\kappa}$, is written as

$$\tilde{\kappa} = \frac{\tilde{h}_{\tilde{x}\tilde{x}}}{(1 + \tilde{h}_{\tilde{x}}^2)^{3/2}}. \tag{2.9}$$

2.1. *Non-dimensional numbers*

In the absence of flow, the combination of gravity and elasticity defines a length scale through the balances of hydrostatic pressure, $\rho g h$, and elastic pressure, $K_B\tilde{\kappa}/l_e^2$,

$$p \sim \rho g h \sim K_B \frac{h}{l_e^4} \Rightarrow l_e = \left(\frac{K_B}{\rho g} \right)^{1/4}. \tag{2.10}$$

We refer to l_e as the elasticity length and is the characteristic scale of the interface in the absence of flow. If the fluid interface is covered by a thin elastic strip, then an elastic meniscus forms in the absence of flow. In a recent study, Rivetti & Antkowiak (2013) determined the shape of an elastic meniscus by covering the fluid interface by a thin elastic strip, the shape of which was also characterized by the elasticity length scale, l_e. As an example of a typical magnitude of K_B, we briefly discuss the result of Vella *et al.* (2004) who determined the Young's modulus and bending stiffness of a particle-laden interface. For rigid particles, Vella *et al.* (2004) suggest that the Young's modulus depends solely on the surface tension, σ, and the particle diameter, d, and is given by

$$E = 2.82\frac{\sigma}{d}. \tag{2.11}$$

Using the relation between bending modulus and Young's modulus (cf. Vella *et al.* 2004), $K_B = Ed^3/12(1-\nu^2)$ where $\nu = 1/\sqrt{3}$ is the Poisson ratio, we obtain

$$K_B = 0.3525\sigma d^2. \tag{2.12}$$

It is of interest to compare this new length to the capillary length, l_c, for clean interfaces governed by a balance of gravity and surface tension.

$$l_e = 0.3525^{1/4}\left(\frac{\sigma d^2}{\rho g}\right)^{1/4} \approx l_c^{1/2} d^{1/2}, \tag{2.13}$$

where the $O(1)$ numerical prefactor has been neglected. Hence, the ratio of l_e/l_c becomes

$$\frac{l_e}{l_c} \approx \left(\frac{d}{l_c}\right)^{1/2} = B_0^{1/4}, \tag{2.14}$$

where B_0 is a Bond number based on the size of the particle. It is clear from the above expression that for small particles, $l_e \ll l_c$.

In the presence of flow, the problem is characterized by the following non-dimensional numbers:

$$\text{Reynolds number,} \quad Re = \frac{\rho U l_e}{\mu}, \tag{2.15a}$$

$$\text{Elasticity number,} \quad El = \frac{\mu U l_e^2}{K_B}. \tag{2.15b}$$

Recall that surface tension effects are neglected in this paper so that a capillary number does not appear. A complete analysis valid for all Re and El is beyond the scope of this paper. We restrict the theory in this paper to the following limiting conditions:

$$El \ll 1 \quad \text{and} \quad ReEl \ll 1. \tag{2.16}$$

For a typical value of $El = 0.1$ and 1 μm-sized particles, we require the velocity of the plate, $U < 1.325$ mm s^{-1}, while for 25 μm-sized particles, we require the plate velocity to be less than 33 mm s^{-1} for the parameters used here.

2.2. *Non-dimensional equations: static region*

We non-dimensionalize the governing equations with the following scales: all length scales by the elasticity length scale, l_e, velocities by plate speed U and pressure with

K_B/l_e^3. The non-dimensional equations then become

$$u_x + v_y = 0, \tag{2.17a}$$

$$ElRe(uu_x + vu_y) = -p_x + El\nabla^2 u - 1, \tag{2.17b}$$

$$ElRe(uv_x + vv_y) = -p_y + El\nabla^2 v, \tag{2.17c}$$

$$u = 1, \quad v = 0 \quad \text{at } y = 0. \tag{2.18}$$

At $y = h(x)$, we have:

$$v - h_x u = 0, \tag{2.19a}$$

$$-p + \frac{2El}{(1+h_x^2)}\left\{u_x(h_x^2 - 1) - (u_y + v_x)h_x\right\} = -\left[\frac{2(1+h_x^2)^2 h_{xxxx} - 20(1+h_x^2)h_x h_{xx} h_{xxx} - 5(1-6h_x^2)h_{xx}^3}{2(1+h_x^2)^{9/2}}\right], \tag{2.19b}$$

$$El[-4u_x h_x + (u_y + v_x)(1 - h_x^2)] = 0. \tag{2.19c}$$

As can be seen from (2.17*b*), (2.17*c*) and (2.19*b*), viscous stresses are negligible for small El. Setting $El = 0$, it is clear from the above equations that the static interface is governed by a balance of gravity and elasticity, with an absence of flow effects as expected. As in the classical Landau–Levich case, the static solution cannot be smoothly matched to the fully developed region near the plate where a film of constant thickness moving at uniform speed exists. Thus, we require a *transition region* near the plate where viscous effects become important and adjust the shape of the interface to match to the fully developed region. In this transition region, the dominant balance is between viscous and elastic forces with gravity being unimportant. We therefore develop the transition layer equations by rescaling all of the variables.

2.3. *Non-dimensional equations: transition region*

In the transition region, a new set of scales are obtained such that viscous forces become as important as the elastic pressure and the equations of motion are given by the lubrication approximation. To obtain the relevant scalings in this region (shown with an overbar), we write

$$(\bar{x}, \bar{y}) = \left(\frac{x}{El^n}, \frac{y}{El^m}\right); \quad \bar{p} = p; \quad (\bar{u}, \bar{v}) = \left(u, \frac{v}{El^{m-n}}\right). \tag{2.20}$$

Balancing the dominant terms in the normal stress balance equation (2.19*b*) and the x-momentum equation (2.17*b*), we find

$$m - 4n = 0, \quad n = 2m - 1, \tag{2.21}$$

which gives $n = 1/7$ and $m = 4/7$. The rescaled variables in the transition region are therefore

$$(\bar{x}, \bar{y}) = \left(\frac{x - x_0}{El^{1/7}}, \frac{y}{El^{4/7}}\right), \tag{2.22a}$$

$$(\bar{u}, \bar{v}) = \left(u, \frac{v}{El^{3/7}}\right), \tag{2.22b}$$

$$\bar{p} = p, \quad \bar{h} = \frac{h}{El^{4/7}}. \tag{2.22c}$$

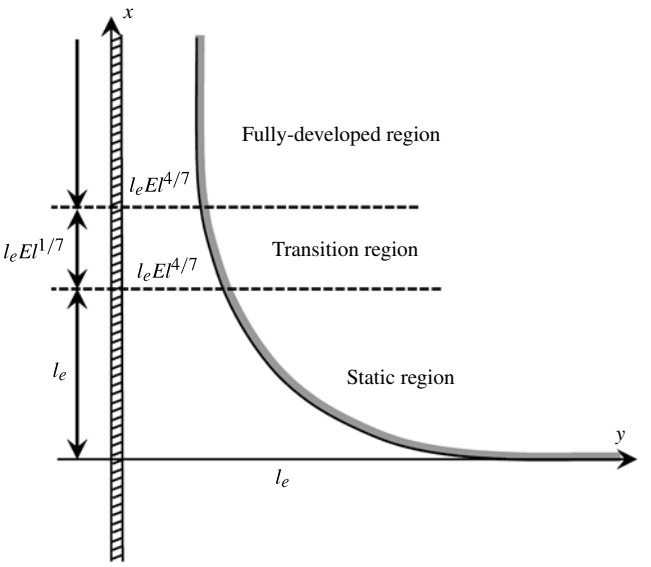

FIGURE 2. The asymptotic structure of the flow showing the breakdown of the problem into three regions: (i) a static region where gravity balances elasticity; (ii) a transition region where the viscous stress balances elasticity; and (iii) a fully developed region where the flow is uniform.

Here x_0 is the origin of the coordinate system the value of which has to be determined as part of the solution procedure. The non-dimensional equations in the transition region in terms of the rescaled variables become

$$\bar{u}_{\bar{x}} + \bar{v}_{\bar{y}} = 0, \tag{2.23a}$$

$$ElRe(\bar{u}\bar{u}_{\bar{x}} + \bar{v}\bar{u}_{\bar{y}}) = -\bar{p}_{\bar{x}} + El^{6/7}\bar{u}_{\bar{x}\bar{x}} + \bar{u}_{\bar{y}\bar{y}} - El^{1/7}, \tag{2.23b}$$

$$ElRe(\bar{u}\bar{v}_{\bar{x}} + \bar{v}\bar{v}_{\bar{y}}) = -\bar{p}_{\bar{y}} + El^{12/7}\bar{v}_{\bar{x}\bar{x}} + El^{6/7}\bar{v}_{\bar{y}\bar{y}}, \tag{2.23c}$$

$$\bar{u} = 1, \quad \bar{v} = 0, \quad \text{at } \bar{y} = 0. \tag{2.24}$$

At $\bar{y} = \bar{h}(\bar{x})$, we have

$$\bar{v} - \bar{h}_{\bar{x}}\bar{u} = 0, \tag{2.25a}$$

$$-\bar{p} + \frac{2El^{6/7}}{\left(1 + El^{6/7}\bar{h}_{\bar{x}}^2\right)}\left[-\bar{h}_{\bar{x}}(\bar{u}_{\bar{y}} + El^{2/7}\bar{v}_{\bar{x}}) - \bar{u}_{\bar{x}} + El^{6/7}\bar{u}_{\bar{x}}\bar{h}_{\bar{x}}^2\right]$$
$$= -\frac{1}{\left(1 + El^{6/7}\bar{h}_{\bar{x}}^2\right)^{9/2}}\left[\bar{h}_{\bar{x}\bar{x}\bar{x}\bar{x}} + O(El^{5/7})\right], \tag{2.25b}$$

$$-4El^{6/7}\bar{u}_{\bar{x}}\bar{h}_{\bar{x}} + \left(\bar{u}_{\bar{y}} + El^{6/7}\bar{v}_{\bar{x}}\right)\left(1 - El^{6/7}\bar{h}_{\bar{x}}^2\right) = 0. \tag{2.25c}$$

Only the leading elastic term is written in the normal stress balance equation in the interest of brevity. In the lubrication approximation, the characteristic scale perpendicular to the plate is much smaller than the scale measured along the plate as reflected in (2.22). We can use $El^{1/7}$ as the relevant small parameter to develop an asymptotic expansion. In terms of this parameter, y scale is three orders smaller than the x scale. This is one of the fundamental differences between the ELL problem and the classical Landau–Levich problem where the y scale is one order smaller

than the x scale in terms of the small parameter, $Ca^{1/3}$. As will be shown later, this mean that: (i) the equation for the interface shape is a highly stiff equation, making the numerics very challenging; (ii) matching the static and transition regions is more complicated; and (iii) higher-order perturbation terms are necessary in order to close the lowest-order problem.

3. Asymptotic expansion and matching conditions

As mentioned above, the nature of the scaling in the transition region suggests that all unknown quantities in both regimes may be expanded in powers of $El^{1/7}$ as follows:

$$h(x) = \sum_{j=0}^{\infty} El^{j/7} h^j(x), \tag{3.1a}$$

$$p(x, y) = \sum_{j=0}^{\infty} El^{j/7} p^j(x, y), \tag{3.1b}$$

$$\boldsymbol{u}(x, y) = \sum_{j=0}^{\infty} El^{j/7} \boldsymbol{u}^j(x, y). \tag{3.1c}$$

For now, we only evaluate the leading-order terms in the expansion. A detailed discussion of higher-order effects is given later.

3.1. *Static region: leading order*

On substituting (3.1) into (2.17)–(2.19), the governing equations in the static region at leading order with $u^{(0)} = v^{(0)} = 0$ become

$$p_x^{(0)} = -1, \tag{3.2a}$$

$$p_y^{(0)} = 0, \tag{3.2b}$$

At $y = h^{(0)}(x)$, we have

$$p^{(0)} - \left[\frac{2\left(1 + (h_x^{(0)})^2\right)^2 h_{xxxx}^{(0)} - 20\left(1 + (h_x^{(0)})^2\right) h_x^{(0)} h_{xx}^{(0)} h_{xxx}^{(0)} - 5\left(1 - 6(h_x^{(0)})^2\right)(h_{xx}^{(0)})^3}{2\left(1 + (h_x^{(0)})^2\right)^{9/2}} \right] = 0. \tag{3.3}$$

The interface far away from the plate has to be nearly flat ($x = 0$) and is determined by the balance of hydrostatic pressure and elasticity. The boundary conditions for the interface shape are given by

$$\left.\begin{aligned} h^{(0)} &\to \infty, \\ h_x^{(0)} &\to -\infty, \\ h_{xx}^{(0)} &\to 0, \\ h_{xxx}^{(0)} &\to 0, \end{aligned}\right\} \quad \text{as } x \to 0. \tag{3.4}$$

The above boundary conditions are not amenable to numerical treatment in their current form. This is due to the difficulty in implementing the first two boundary conditions of (3.4). In § 4 below, we obtain the solution of the static problem by switching the coordinate system.

3.2. *Transition region: leading order*

On substituting (3.1) into (2.23)–(2.25), the governing equations in the transition region at leading order become

$$\bar{u}^{(0)}_{\bar{x}} + \bar{v}^{(0)}_{\bar{y}} = 0, \tag{3.5a}$$

$$\bar{p}^{(0)}_{\bar{x}} = \bar{u}^{(0)}_{\bar{y}\bar{y}}, \tag{3.5b}$$

$$\bar{p}^{(0)}_{\bar{y}} = 0, \tag{3.5c}$$

$$\bar{u}^{(0)} = 1, \quad \bar{v}^{(0)} = 0 \quad \text{at } \bar{y} = 0. \tag{3.6}$$

At $\bar{y} = \bar{h}^{(0)}(\bar{x})$, we have

$$\bar{u}^{(0)}\bar{h}^{(0)}_{\bar{x}} - \bar{v}^{(0)} = 0, \tag{3.7a}$$

$$\bar{p}^{(0)} - \bar{h}^{(0)}_{\bar{x}\bar{x}\bar{x}\bar{x}} = 0, \tag{3.7b}$$

$$\bar{u}^{(0)}_{\bar{y}} = 0. \tag{3.7c}$$

A parabolic velocity field is obtained in the usual way by integrating the x momentum equation

$$\bar{u}^{(0)} = \bar{p}^{(0)}_{\bar{x}} \left(\frac{\bar{y}^2}{2} - \bar{h}\bar{y} \right) + 1. \tag{3.8}$$

By using conservation of mass and eliminating $\bar{p}^{(0)}$, a nonlinear differential equation can be derived for the film thickness, $\bar{h}^{(0)}(\bar{x})$,

$$\bar{h}^{(0)}_{\bar{x}\bar{x}\bar{x}\bar{x}\bar{x}} = \frac{3\left(\bar{h}^{(0)} - \bar{h}^{(0)}_{\infty}\right)}{\left(\bar{h}^{(0)}\right)^3}. \tag{3.9}$$

This equation is analogous to the classical Landau–Levich equation and we refer to it as the ELL equation. We discuss its numerical solution later; here we focus on the asymptotic behaviour for large positive and negative $\bar{x}$ respectively.

In order to match the solution of the above equation to the thin-film region, we require $\bar{h} \to \bar{h}_{\infty}$ as $\bar{x} \to \infty$. Linearizing (3.9) about the fully developed film thickness results in a quintic characteristic equation. Of its five roots, only the two decaying roots are physically relevant. Therefore, the far-field condition becomes

$$\bar{h}^{(0)} = \bar{h}^{(0)}_{\infty} + \mathrm{e}^{\lambda_r \bar{x}}\{A\cos(\lambda_i \bar{x}) + B\sin(\lambda_i \bar{x})\} \quad \text{as } \bar{x} \to \infty, \tag{3.10}$$

where $\lambda_r < 0$ and A, B are arbitrary constants. The eigenvalue, λ, depends on the film thickness and is given by

$$\lambda_r + \mathrm{i}\lambda_i = \frac{3^{1/5}}{\bar{h}_{\infty}^{3/5}} \left[\cos\left(\frac{4\pi}{5}\right) + \mathrm{i}\sin\left(\frac{4\pi}{5}\right) \right]. \tag{3.11}$$

We can absorb the constant B into an arbitrary choice of the origin. Thus, the above asymptotic behaviour simplifies to

$$\bar{h}^{(0)} = \bar{h}^{(0)}_{\infty} + A\mathrm{e}^{\lambda_r \bar{x}}\cos(\lambda_i \bar{x}) \quad \text{as } \bar{x} \to \infty. \tag{3.12}$$

Here both A and $\bar{h}_{\infty}$ are unknown and have to be determined.

As $\bar{x}$ becomes large and negative, the film thickness goes to infinity. From (3.9), it is easy to see that the interface shape assumes a simple quartic form:

$$\bar{h}^{(0)} = c_0\bar{x}^4 + c_1\bar{x}^3 + c_2\bar{x}^2 + c_3\bar{x} + c_4. \tag{3.13}$$

Similarly, the constants c_i are unknown at this stage and have to be determined by matching to the static equations.

3.3. *The matching conditions*

To continue the analysis further, the solution in the transition region has to be matched with the solution of the static region (discussed below). Using (2.22), the matching condition can be written as

$$\lim_{\bar{x}\to-\infty} El^{4/7}\bar{h}(\bar{x}) = \lim_{x\to x_0} h(x), \tag{3.14}$$

where the limits are interpreted in the spirit of the matching principle of Van Dyke (1975). Expanding $h(x)$ about $x = x_0$ using Taylor series, the matching conditions for $h^{(0)}$ and $h^{(1)}$ become

$$O(El^{(0)}): \quad h^{(0)}(x_0) = 0, \tag{3.15}$$

$$O(El^{1/7}): \quad h_x^{(0)}(x_0) = 0, \tag{3.16a}$$

$$h^{(1)}(x_0) = 0, \tag{3.16b}$$

$$O(El^{2/7}): \quad h_{xx}^{(0)}(x_0) = 0, \tag{3.17a}$$

$$h_x^{(1)}(x_0) = 0, \tag{3.17b}$$

$$O(El^{3/7}): \quad h_{xxx}^{(0)}(x_0) = 0, \tag{3.18a}$$

$$h_{xx}^{(1)}(x_0) = 0, \tag{3.18b}$$

$$O(El^{4/7}): \quad h_{xxxx}^{(0)}(x_0) = 24c_0, \tag{3.19a}$$

$$h_{xxx}^{(1)}(x_0) = 6c_1. \tag{3.19b}$$

Since the static region does not perceive the presence of a thin film in the inner region near the plate, $x = x_0$ is the location of the contact line where the static interface meets the vertical plate. Recall that x_0 is unknown and has to be determined as part of the solution of the static equations. According to the above matching conditions (3.16*a*), (3.17*a*) and (3.18*a*), the leading-order static interface meets the vertical plate with zero contact angle, zero curvature and zero moment.

4. Static (outer) region: solution

We now obtain the shape of the static interface far from the plate. In this region, elasticity balances gravity and the interface shape is governed by (3.3). Since the boundary conditions are inhomogeneous as $x \to 0$, it is difficult to solve the static equations in the current coordinate system. Instead, we switch the coordinate system by assuming a one-to-one map from (x, h) plane to (η, ξ) plane as shown schematically in figure 3. Eliminating pressure, the static equation for the interface height, $\eta(\xi)$, in the switched coordinate axes becomes

$$\eta_{\xi\xi\xi\xi} = -\eta\left(1+\eta_\xi^2\right)^{5/2} + \frac{10\eta_\xi\eta_{\xi\xi}\eta_{\xi\xi\xi}}{\left(1+\eta_\xi^2\right)} + \frac{5\left(1-6\eta_\xi^2\right)\eta_{\xi\xi}^3}{2\left(1+\eta_\xi^2\right)^2}, \tag{4.1}$$

with $\eta \to 0$ as $\xi \to \infty$. The solution η can be expanded in powers of $El^{1/7}$ as

$$\eta = \eta^{(0)} + El^{1/7}\eta^{(1)} + O(El^{2/7}). \tag{4.2}$$

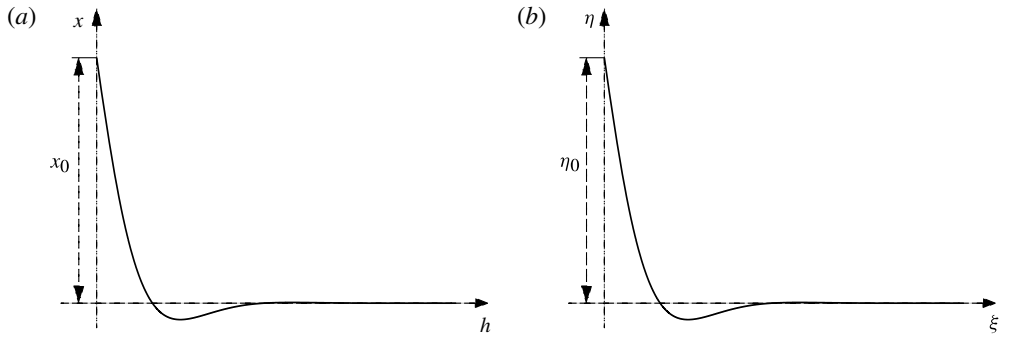

FIGURE 3. Transformation from the original (x, h) axes to (η, ξ) axes.

4.1. *The $O(1)$ static solution*

The equation for the leading-order term $\eta^{(0)}$ is identical to (4.1) and we do not repeat it here. We now consider the solution to the static problem at the leading order. Linearizing this equation about $\eta = 0$, the far-field boundary condition becomes

$$\eta^{(0)} = \mathrm{e}^{\lambda_r \xi}\{a\cos(\lambda_i \xi) + b\sin(\lambda_i \xi)\}, \tag{4.3}$$

where a and b are arbitrary constants and $\lambda_r \pm \mathrm{i}\lambda_i = (1 \pm \mathrm{i})/\sqrt{2}$. Eliminating a and b, two boundary or consistency conditions can be obtained:

$$\left.\begin{aligned} \eta^{(0)}_{\xi\xi} &= -\eta^{(0)} + 2\lambda_r \eta^{(0)}_{\xi} \\ \eta^{(0)}_{\xi\xi\xi} &= -\eta^{(0)}_{\xi} + 2\lambda_r \eta^{(0)}_{\xi\xi} \end{aligned}\right\} \quad \text{as } \xi \to \infty. \tag{4.4}$$

In order to obtain additional boundary conditions, we examine the region close to the plate. As shown in figure 3, x_0 is mapped to a the point η_0 on the plate. From the matching conditions in § 3.3, since $h_{xxxx} = 24c_0$ and all lower derivatives are zero, we require in the vicinity of the contact line $x = x_0$ that

$$h^{(0)} = c_0(x - x_0)^4 \quad \text{near } x = x_0. \tag{4.5}$$

In term of $\eta^{(0)}$ and ξ, we have

$$\xi = c_0(\eta^{(0)} - \eta_0)^4. \tag{4.6}$$

Defining $d = c_0^{-1/4}$, rewriting the above result as an equation for $\eta^{(0)}$ and differentiating, we have

$$\eta^{(0)} = \eta_0 + d\xi^{1/4}, \tag{4.7a}$$

$$\eta^{(0)}_{\xi} = \frac{d}{4}\xi^{-3/4}, \tag{4.7b}$$

$$\eta^{(0)}_{\xi\xi} = -\frac{3d}{16}\xi^{-7/4}, \tag{4.7c}$$

$$\eta^{(0)}_{\xi\xi\xi} = \frac{21d}{64}\xi^{-11/4}, \tag{4.7d}$$

$$\eta^{(0)}_{\xi\xi\xi\xi} = -\frac{231d}{256}\xi^{-15/4}. \tag{4.7e}$$

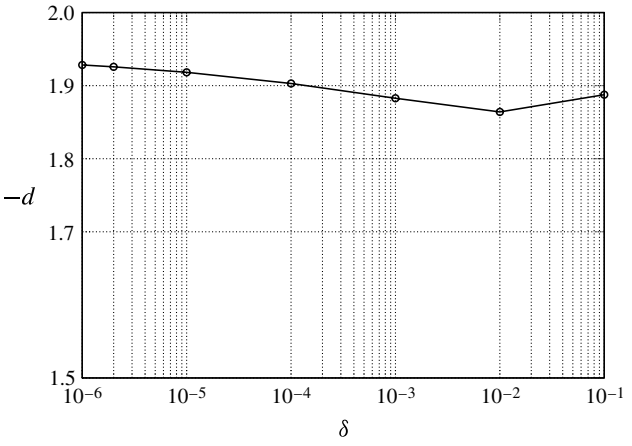

FIGURE 4. Variation of parameter d in (4.7) with δ.

The above expressions are consistent with the singular nature of the boundary conditions as $\xi \to 0$. Substituting (4.7) into (4.1) and balancing the dominant terms as $\xi \to 0$, we get the simple result

$$\eta_0 = \frac{24}{d^4}. \tag{4.8}$$

Since η_0 is still unknown, we solve (4.1) as a boundary value problem (BVP) with two boundary conditions, (4.4), in the far field and three boundary conditions, (4.7), near $\xi = 0$. Owing to the singular nature of the problem near the plate, we apply the boundary condition at $\xi = \delta$ with $\delta \ll 1$. For numerical purposes, we sequentially decrease the size of δ starting from 0.1, each time using the solution for larger δ to improve the accuracy of the solution. The parameter d in (4.7) is negative and converges with decreasing δ as shown in figure 4. Using a value of $d = -1.928$ at $\delta = 10^{-6}$, we get the contact line position as $\eta_0 = 1.735$. In dimensional units, the contact line position is $1.735 l_e$ where l_e is the elasticity length scale. For purpose of comparison, a static interface governed by a balance of surface tension and gravity rises to a height of $\sqrt{2} l_c$ where l_c is the capillary length scale (see Park 1991). The shape of the elastic interface with $\delta = 10^{-6}$ is shown in figure 5. Clearly, an elastic interface exhibits an oscillatory structure. Although the exact shape of the interface would change with the specific elasticity model employed, the oscillatory structure would exist for all elastic interfaces. The shape of the elastic meniscus studied here is similar to a recent study by Rivetti & Antkowiak (2013) in which a static interface was covered by a thin elastic strip. Direct comparison with their results is not possible owing to the different elasticity model used.

Finally, the leading coefficient of the quartic polynomial in (3.13) is

$$c_0 = \frac{1}{d^4} = 0.0723. \tag{4.9}$$

This provides one boundary condition for the solution of (3.9). A second boundary condition is required and is obtained by examining higher-order corrections to the static problem.

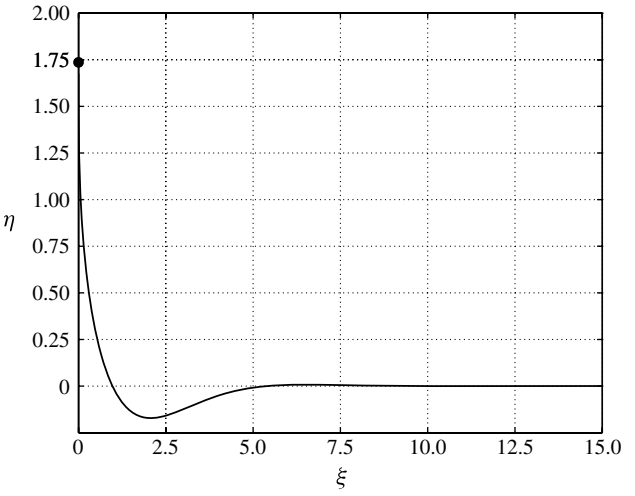

FIGURE 5. Shape of an elastic interface with $\delta = 10^{-6}$. The symbol shows the location of the contact line at $\eta_0 = 1.735$.

4.2. *The $O(El^{1/7})$ correction*

In this subsection, we will examine higher-order terms in the static problem. Expanding η in (4.1) in powers of $El^{1/7}$, a linear homogeneous equation for $\eta^{(1)}$ is obtained:

$$\eta^{(1)}_{\xi\xi\xi\xi} + M_1\eta^{(1)}_{\xi\xi\xi} + M_2\eta^{(1)}_{\xi\xi} + M_3\eta^{(1)}_{\xi} + M_4\eta^{(1)} = 0, \tag{4.10}$$

where the coefficients M_1–M_4 are functions of ξ and depend on the leading-order solution, $\eta^{(0)}$. The expressions for these coefficients are given in Appendix. Near $\xi = 0$, based on the matching conditions in § 3.3, we again expect $\eta^{(1)}$ to have a power-law dependence on ξ as follows:

$$\eta^{(1)} = \eta_1 + F\xi^a, \tag{4.11a}$$

$$\eta^{(1)}_{\xi} = aF\xi^{a-1}, \tag{4.11b}$$

$$\eta^{(1)}_{\xi\xi} = a(a-1)F\xi^{a-2}, \tag{4.11c}$$

$$\eta^{(1)}_{\xi\xi\xi} = a(a-1)(a-2)F\xi^{a-3}, \tag{4.11d}$$

$$\eta^{(1)}_{\xi\xi\xi\xi} = a(a-1)(a-2)(a-3)F\xi^{a-4}. \tag{4.11e}$$

Here η_1 is the first-order correction to the position of the contact line and $a > 0$ to ensure regularity of $\eta^{(1)}$. Substituting (4.11) into (4.10) and using (4.7) near $\xi = 0$, we get the following expression (after taking the limit $\xi \to 0$):

$$\left(864a - 704a^2 - 1536a^3 - 1024a^4\right)F + d^5\left(\eta_1\xi^{-15/4} + F\xi^{a-15/4}\right) = 0. \tag{4.12}$$

Since $\xi^{-15/4} \to \infty$ as $\xi \to 0$, we set $\eta_1 = 0$. Physically, this shows that there is no correction to the position of the contact line at this order. For the above equation to the satisfied independent of the value of ξ, we further require $F = 0$. Hence from (4.11), the first-order correction vanishes identically. The same result can be established from the following fact: the static (4.1) is correct up to $O(El^{4/7})$. Viscous terms becomes important beyond this order. Hence any correction to the solution of

the static problem has to arise from modifications to the boundary conditions. Since the origin of the coordinate system moves with the interface, we can argue that the origin $x = x_0$, and hence η_0, is independent of El. Therefore, first-order corrections cannot arise in the present problem. The important consequence follows from the matching conditions (3.19): we require $h^{(1)}_{xxx}(x_0) \equiv 0$, and therefore $c_1 = 0$.

5. Transition (inner) region: solution

Having obtained the values of c_0 and c_1, we are now in a position to solve the ELL equation (3.9). Recall that both A and $\bar{h}_\infty$ in the boundary condition (3.12) are unknown. Using the far-field quartic behaviour of $\bar{h}(\bar{x})$ from (3.13), we have

$$\frac{\bar{h}^{(0)}_{\bar{x}\bar{x}\bar{x}}}{\bar{h}^{(0)}_{\bar{x}\bar{x}\bar{x}\bar{x}}} = \bar{x} + \frac{c_1}{4c_0}, \\ = \bar{x} + I, \tag{5.1}$$

where I is the intercept. Combining these, we have

$$\bar{h}^{(0)}_{\bar{x}\bar{x}\bar{x}\bar{x}\bar{x}} = \frac{3\left(\bar{h}^{(0)} - \bar{h}^{(0)}_\infty\right)}{\left(\bar{h}^{(0)}\right)^3}, \tag{5.2a}$$

with

$$\bar{h}^{(0)} = \bar{h}^{(0)}_\infty + A\mathrm{e}^{\lambda_r \bar{x}}\cos(\lambda_i \bar{x}) \quad \text{and its derivatives as } \bar{x} \to \infty, \tag{5.2b}$$

$$\left.\begin{aligned} \bar{h}^{(0)}_{\bar{x}\bar{x}\bar{x}\bar{x}} &= 24c_0, \\ \frac{\bar{h}^{(0)}_{\bar{x}\bar{x}\bar{x}}}{\bar{h}^{(0)}_{\bar{x}\bar{x}\bar{x}\bar{x}}} &= \bar{x} + I, \end{aligned}\right\} \quad \text{as } \bar{x} \to -\infty. \tag{5.2c}$$

With five boundary conditions from (5.2*b*) and two from (5.2*c*), we have a total of seven boundary conditions to solve for the interface shape, $\bar{h}(\bar{x})$, and the unknowns A and $\bar{h}_\infty$. This completes the formulation of the problem. Since (5.2*a*) is translationally invariant, it can easily be shown from (5.2*b*) that

$$\bar{h}^{(0)}(\bar{x}; A) = \bar{h}^{(0)}\left(\bar{x} + \frac{2\pi}{\lambda_i}; A\exp\left[\frac{-2\pi\lambda_r}{\lambda_i}\right]\right). \tag{5.3}$$

For numerical purposes, we fix the upper limit of the integration domain to $\bar{x}_{max} = 0$ and the lower limit to $\bar{x}_{min} = -100$ in all of the numerical calculations. With guessed values for A and $\bar{h}_\infty$, we solve (5.2*a*) as an initial value problem (IVP), with (5.2*b*) serving as the initial values. We then iteratively solve for $\bar{h}_\infty$ such that the first condition in (5.2*c*) is satisfied. By sequentially changing the value of A, we obtain a family of solutions in the $A - \bar{h}_\infty$ plane. We then use the second condition in (5.2*c*) to determine the value of $\bar{h}_\infty$ for which the intercept vanishes. Figure 6 shows the variation of intercept, I, with the parameter A for one set of IVP calculations. In the vicinity of $I = 0$, the intercept, I, and film thickness, $\bar{h}_\infty$, vary as

$$I = 1.4909 \times 10^4 A - 2.854, \tag{5.4}$$

$$\bar{h}^{(0)}_\infty = 1010A + 0.0587. \tag{5.5}$$

The zero-crossing of I occurs at $A = 2.026 \times 10^{-4}$ and the value of the film thickness at $I = 0$ is $\bar{h}_\infty = 0.2634$.

Since (5.2*a*) is a highly stiff equation, we verify the validity of the IVP solution with a BVP approach. Since $c_1 = 0$, using the far field quartic behaviour of $\bar{h}^{(0)}(\bar{x})$

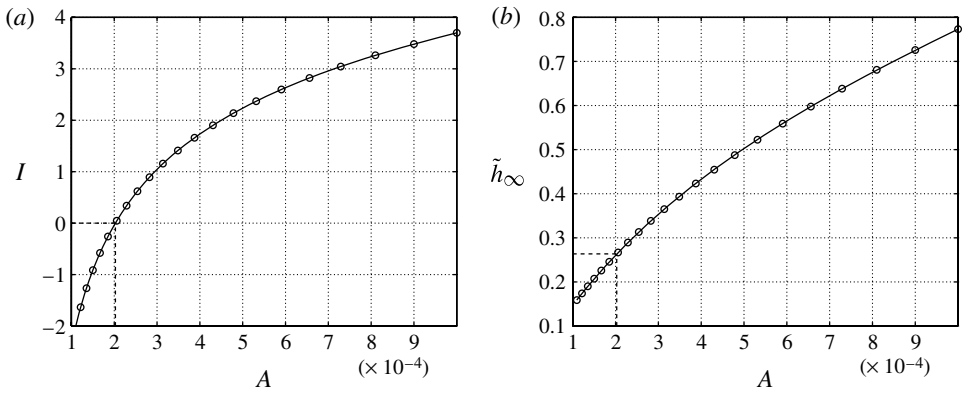

FIGURE 6. Variation of (*a*) intercept, I, and (*b*) film thickness, $\bar{h}_\infty$, as a function of the parameter A using an IVP approach. Every point on the curve satisfies the first condition in (5.2*c*) and the dashed lines show the location of the solution which also satisfies the second condition in (5.2*c*) with $I = 0$.

Solution	A	$\bar{h}_\infty^{(0)}$
1	2.007×10^{-12}	0.0999
2	-1.7777×10^{-10}	0.1157
3	1.6483×10^{-8}	0.1390
4	-1.6594×10^{-6}	0.1783
5	2.0258×10^{-4}	0.2634

TABLE 1. List of solutions obtained by solving (3.9) using a BVP approach.

from (3.13), we have

$$\left.\begin{aligned} \bar{h}^{(0)}_{\bar{x}\bar{x}\bar{x}\bar{x}} &= 24c_0, \\ \bar{h}^{(0)}_{\bar{x}\bar{x}\bar{x}} &= 24c_0\bar{x}_{min}, \end{aligned}\right\} \quad \text{at } \bar{x} = \bar{x}_{min}. \tag{5.6}$$

We can solve (5.2*a*) as a BVP with five boundary conditions, (5.2*b*), at $\bar{x}_{max} = 0$ and two boundary conditions, (5.2*c*), at $\bar{x}_{min} = -100$. To solve the BVP, we first solve an IVP with a guess value for A and $\bar{h}_\infty$. This IVP solution is used as the starting guess solution for the BVP solver. We use MATLAB's *bvp4c* solver in all of the calculations. The parameters A and $\bar{h}_\infty$ were varied in the ranges $[10^{-10}, 10^{-2}]$ and $[0.1, 2.5]$, respectively, and show excellent agreement with the solution obtained from the IVP approach discussed above.

Remarkably, we find multiple solutions, i.e. pairs of $(A, \bar{h}_\infty)$ that satisfy all of the conditions, unlike the classical Landau–Levich flow where the solution is unique. Table 1 gives the values of $(A, \bar{h}_\infty)$ for these five solutions. Although these were the only solutions found using above ranges for A and $\bar{h}_\infty^{(0)}$, it does not rule out the possibility of solutions with other values of $\bar{h}_\infty^{(0)}$. Each of the solutions given in table 1 have been verified with the IVP approach. The five branches of solutions can be written in dimensional form as

$$\tilde{h}^{(0)}_{\infty,e} = \bar{h}^{(0)}_\infty l_e E l^{4/7}. \tag{5.7}$$

where $\bar{h}_\infty$ takes any one of the values given in table 1. Equation (5.7) is the main result of this paper, as it establishes the relationship between the film thickness and a combination of physical properties and dynamic conditions. In particular, since $El = \mu U l_e^2/K_B$, the film thickness varies with the plate speed as $U^{4/7}$.

Equation (5.7) is also to be compared and contrasted with the classical result for a clean interface,

$$\tilde{h}_{\infty,c} = 0.9458 l_c Ca^{2/3} \tag{5.8}$$

One notes that the capillary and elastic length scales play analogous roles in the two theories, and that while the leading constant is unique in the classical case, we have discovered multiple solutions, and hence several values of the leading constant ($\bar{h}_\infty$), in the elastic case. Finally, we note that the dependence on the plate speed, U, differs slightly in the two cases: $U^{2/3}$ in the classical case as compared with $U^{4/7}$ in the elastic case. This difference is discussed below in the context of the experiments of Ouriemi & Homsy (2013).

The non-uniqueness of the solution is remarkable but not surprising. Equation (3.9) is a complex nonlinear BVP, and hence it is possible that multiple solutions exist. A classic example of a similar scenario is the existence of a continuous family of solutions to the Saffman–Taylor fingering problem (see Saffman & Taylor 1958). Inclusion of surface tension by McLean & Saffman (1981) changes the nature of solutions from an continuous family to a discrete set resulting in multiple values for the finger width. Another example is the existence of multiple solutions for the shape of a rising inviscid bubble in a two-dimensional channel (see Vanden-Broeck 1984). Interestingly, in this case, the solution becomes unique in the limit of vanishing surface tension. The non-uniqueness may be resolved through stability analysis of the discrete set of solutions: we leave stability analysis for future study and do not pursue the matter here.

Figure 7(*a*) shows the structure of the flow field for the case with $\bar{h}_\infty^{(0)} = 0.2634$. Using (3.8), it can be shown that there exists an interfacial stagnation point at $\bar{y} = \bar{h}_s = 3\bar{h}_\infty^{(0)}$. This is identical to the classical Landau–Levich case. In addition to the stagnation point, there exists a 'dimple' where the film thickness is at its minimum. This is consistent with (3.12) which shows that the film thickness follows an oscillatory decay into the thin-film region. Snoeijer *et al.* (2008) recently found such 'dimpled' solutions even in the classical Landau–Levich flow, but for cases when the plate was partially wetting. Figure 7(*b*) shows the variation of the pressure gradient along the interface. For comparison, we also plot the pressure gradient in the classical Landau–Levich flow. As the interface curvature changes sign, a large adverse pressure gradient is generated with a minimum at the location of the dimple. Note that the variations in the pressure gradients is much larger in the present problem compared with the classical Landau–Levich flow. This could have important implications for the transport of particles along the interface for cases when the particles are not in a jammed state.

6. Discussion

In this paper, we have developed a theory of dip-coating flow governed by interfacial elasticity rather than surface tension. In analogy with the classical Landau–Levich dip-coating flow, we call this the ELL flow. To model elasticity of the interface, we take recourse to the widely used Helfrich model of elasticity and our analysis is valid for small elasticity number. A scaling analysis reveals the presence

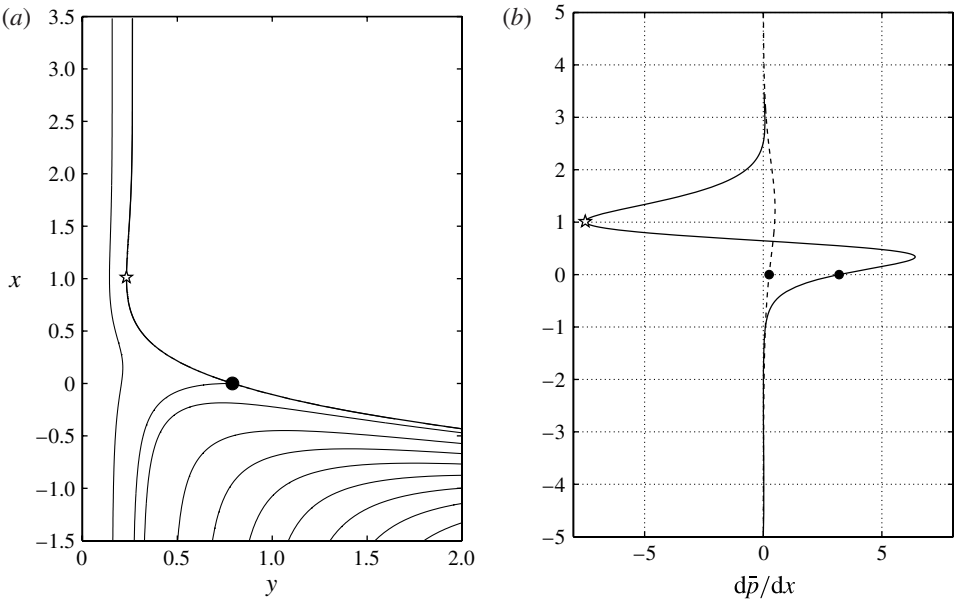

FIGURE 7. (*a*) Flow field showing the location of the stagnation point (●) and the dimple (☆). (*b*) Comparison of pressure gradient distribution with elasticity (solid) with the Landau–Levich case (dashed).

of two regions near the plate: a static or outer region governed by the balance of elasticity and gravity, and a transition or inner region governed by a balance of elasticity and viscous forces. An asymptotic expansion in powers of $El^{1/7}$ is developed in the two regions. There are a number of differences between an ELL flow and the classical Landau–Levich flow owing to the higher-order derivative terms as a result of elasticity. (i) In the classical Landau–Levich flow, the static meniscus shape can be found independent of the matching conditions and the solution has an non-oscillatory structure, whereas in the ELL, matching conditions are needed to generate the necessary boundary conditions for the static problem and the interface shape has an oscillatory structure. (ii) In the classical Landau–Levich flow, the curvature (and hence pressure) of the outer solution is non-zero at the apparent contact line whereas in the ELL, both curvature and moment are zero there. (iii) In the ELL flow, higher-order terms in the static problem are required to close the leading-order problem in the transition region, unlike the classical Landau–Levich flow.

It is shown that the film thickness scales as $El^{4/7}$, or in terms of the plate velocity as $U^{4/7}$. As mentioned in the introduction, the present work was motivated in part from the experiments of Ouriemi & Homsy (2013) where an experimental study was carried out to determine the effect of surface-adsorbed hydrophobic particles on dip-coating flows. It is interesting to note that at high surface concentration of particles, these authors find that the film thickness scales as $Ca^{0.57}$, or in terms of the velocity, as $U^{0.57}$. This is identical to the scaling found in the present study suggesting that elasticity may have had a role in their results.

In Ouriemi & Homsy (2013), the film thickness was non-dimensionalized by the capillary length scale and its variation was plotted as a function of capillary number. To convert these results to the elasticity length scale and elasticity number, we

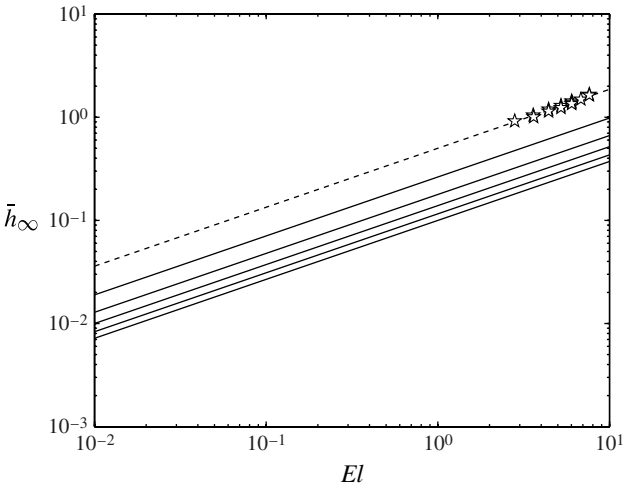

FIGURE 8. Comparison of the present theory with the experiments of Ouriemi & Homsy (2013). The symbols show the experimental results, solid lines show the theoretical predictions from (5.7) for each of the multiple solutions and the dashed line is an approximate fit to the experimental data (see the text for more details).

need an estimation of the ratios l_e/l_c and El/Ca. Two types of particles were used in the dip-coating experiments: fingerprint powder with a typical particle size of $d \approx 1$ μm, and polystyrene particles with $d \approx 25$ μm. The fluid used was a solution of NaCl with $\sigma = 0.076$ N m^{-1}, $\rho = 1056$ kg m^{-3} and $\mu = 1.25 \times 10^{-3}$ Pa s. With particles of $d = 1$ μm, using (2.10) and (2.12), we get $K_B = 2.679 \times 10^{-14}$ N m and $l_e \approx 4 \times 10^{-5}$ m $= 40$ μm. And with particles with $d = 25$ μm, we get $K_B = 1.674 \times 10^{-11}$ N m and $l_e \approx 2 \times 10^{-4}$ m $= 20$ μm. Upon expressing l_e and El in (5.7) in terms of fundamental parameters of the problem, it can be verified that the film thickness varies with the bending stiffness as $K_B^{-1/28}$. This dependence is surprisingly weak given that interface bending is the only physical parameter controlling the mechanical property of the interface. Comparing l_e to the capillary length, which has a value of $l_c = 2.7 \times 10^{-3}$ m, it is clearly evident that the elasticity length scale is much smaller than the capillary length scale for these range of particle sizes. In the case of fingerprint power ($d = 1$ μm), we estimate

$$\frac{l_e}{l_c} \approx 0.0148, \tag{6.1}$$

and

$$\frac{El}{Ca} \approx 4.5 \times 10^3. \tag{6.2}$$

In the experiments, the capillary number approximately ranges from 6×10^{-4} to 1.7×10^{-3}. Therefore, the elasticity number varies from 2.80 to 7.63. Clearly the experiments do not fall into the small El regime investigated in the present paper. However, the coincidence in the power laws invites further comparison. Figure 8 shows a comparison of the experimentally obtained film thickness, scaled by l_e, and

the present theoretical prediction. The dashed line shows an approximate fit given by $h_\infty = 0.5El^{4/7}$, i.e. the experimental data approximately differs by a factor of two from the highest film thickness obtained in table 1. There could be a number of reasons for the discrepancy between experiments and the present theory. (i) The experimental results do not fall into the small El regime required to apply the present theory. (ii) The prediction of Vella *et al.* (2004) could underestimate the bending stiffness of the particle-laden interface. However, given the weak dependence of the film thickness on the bending stiffness would require a large change in the value of K_B from that estimated above in order to account for the factor of 2.0. (iii) Surface tension effects, neglected in the present paper, could be important.

As discussed in the introduction, it is necessary to sound a note of caution regarding the direct applicability of the present theory to experiments with particles. Several reasons for this have already been discussed and are amplified below. However, the present analysis is the first to consider the effect of bending stiffness on coating flows. As such, it provides a benchmark and is an appropriate first step in developing a more complete understanding of interfacial elasticity. The present theory can be extended in a number of different directions. In a companion paper, we investigate the effect the combined effects of elasticity and surface tension on dip-coating flows. In addition, when the particles are not in a jammed state, it is conceivable that the particle concentration will vary along the interface. In such a case, elasticity will not be constant but will also vary along the interface. The effect of variable elasticity will lead to generation of tangential stresses along the interface giving rise to Marangoni-like stress terms. The present theory can also be applied to other geometries, especially for situations similar to the Bretherton problem. This could be of interest in the biological context where walls of the tube possess elasticity. Finally, we mention the issue of non-uniqueness of the solutions. As discussed before, a detailed stability analysis might shed more light on this issue and could even resolve it. We leave this for future work.

Acknowledgements

HND thanks Ian Hewitt and Neil Balmforth for many fruitful discussions. We gratefully acknowledge funding from the Natural Science and Engineering Research Council (NSERC) of Canada.

Appendix. Coefficients M_1–M_4 in (4.10)

Here we give the coefficients M_1–M_4 in (4.10):

$$M_1 = -\frac{10\eta_\xi^{(0)}\eta_{\xi\xi}^{(0)}}{1+\left(\eta_\xi^{(0)}\right)^2}, \tag{A 1}$$

$$M_2 = -\left[\frac{15\left(1-6\left(\eta_\xi^{(0)}\right)^2\right)\left(\eta_{\xi\xi}^{(0)}\right)^2}{2\left(1+\left(\eta_\xi^{(0)}\right)^2\right)^2} + \frac{10\eta_\xi^{(0)}\eta_{\xi\xi\xi}^{(0)}}{1+\left(\eta_\xi^{(0)}\right)^2}\right], \tag{A 2}$$

$$M_3 = 5\eta^{(0)}\eta_\xi^{(0)}\left(1+\left(\eta_\xi^{(0)}\right)^2\right)^{3/2} + \frac{10\eta_\xi^{(0)}\left(4-3\left(\eta_\xi^{(0)}\right)^2\right)\left(\eta_{\xi\xi}^{(0)}\right)^3}{\left(1+\left(\eta_\xi^{(0)}\right)^2\right)^3} - \frac{10\left(1-\left(\eta_\xi^{(0)}\right)^2\right)\eta_{\xi\xi}^{(0)}\eta_{\xi\xi\xi}^{(0)}}{\left(1+\left(M_\xi\right)^2\right)^2} \tag{A 3}$$

$$M_4 = \left(1+\left(\eta_\xi^{(0)}\right)^2\right)^{5/2}. \tag{A 4}$$

REFERENCES

AUDOLY, B. 2011 Localized buckling of a floating elastica. *Phys. Rev.* E **84**, 011605.

AUSSILLOUS, P. & QUÉRÉ, D. 2001 Liquid marbles. *Nature* **411**, 924–927.

BINKS, B. P. 2002 Particles as surfactants - similarities and differences. *Curr. Opin. Colloid Interface Sci.* **7**, 21–41.

BRETHERTON, F. P. 1961 The motion of long bubbles in tubes. *J. Fluid Mech.* **10**, 166–188.

CAMPANA, D. M., UBAL, S., GIAVEDON, M. D. & SAITA, F. A. 2010 Numerical prediction of the film thickening due to surfactants in the Landau–Levich problem. *Phys. Fluids* **22**, 032103.

CAMPANA, D. M., UBAL, S., GIAVEDON, M. D. & SAITA, F. A. 2011 A deeper insight into the dip coating process in the presence of insoluble surfactants: a numerical analysis. *Phys. Fluids* **23**, 052102.

CHAN, D. Y. C., HENRY, J. D. Jr. & WHITE, L. R. 1981 The interaction of colloidal particles collected at a fluid interface. *J. Colloid Interface Sci.* **79**, 410–418.

DAICIC, J., FOGDEN, A., CARLSSON, I., WENNERSTRÖM, H. & JÖNSSON, B. 1996 Bending of ionic surfactant monolayers. *Phys. Rev.* E **54**, 3984–3998.

DANOV, K. D. & KRALCHEVSKY, P. A. 2010 Capillary forces between particles at a liquid interface: general theoretical approach and interactions between capillary multipoles. *Adv. Colloid Interface Sci.* **154**, 91–103.

DERJAGUIN, B. V. 1943 On the thickness of the liquid film adhering to the walls of a vessel after emptying. *Acta Physicochim. USSR* **20**, 349–352.

DIAMANT, H. & WITTEN, T. A. 2011 Compression induced folding of a sheet: an integrable system. *Phys. Rev. Lett.* **107**, 164302.

DINSMORE, A. D., HSU, M. F., NIKOLAIDES, M. G., MARQUEZ, M., BAUSCH, A. R. & WEITZ, D. A. 2002 Colloidosomes: selectively permeable capsules composed of colloidal particles. *Science* **298**, 1006–1009.

FAINERMAN, V. B., KOVALCHUK, V. I., LUCASSEN-REYNDERS, E. H., GRIGOURIEV, D. O., FERRI, J. K., LESER, M. E., MICHEL, M., MILLER, R. & MÖHWALD, H. 2006 Surface-pressure isotherms of monolayers formed by microsize and nanosize particles. *Langmuir* **22**, 1701–1705.

FULLER, G. G. & VERMANT, J. 2012 Complex fluid–fluid interfaces: rheology and structure. *Ann. Rev. Chem. Biomol. Engng* **3**, 519–543.

GASKELL, P. H., SAVAGE, M. D., SUMMERS, J. L. & THOMPSON, H. M. 1995 Modelling and analysis of meniscus roll coating. *J. Fluid Mech.* **298**, 113–137.

GAVER, D. P. III, HALPERN, D., JENSEN, O. E. & GROTBERG, J. B. 1996 The steady motion of a semi-infinite bubble through a flexible-walled channel. *J. Fluid Mech.* **319**, 25–65.

GAVER, D. P. III, SAMSEL, R. W. & SOLWAY, J. 1990 Effects of surface tension and viscosity on airway reopening. *J. Appl. Physiol.* **69**, 74–85.

GIFFORD, W. A. & SCRIVEN, L. E. 1971 On the attraction of floating particles. *Chem. Engng Sci.* **26**, 287–297.

GROENVELD, P. 1970*a* Dip-coating by withdrawal of liquid films. PhD thesis, Delft University.

GROENVELD, P. 1970*b* Low capillary number withdrawal. *Chem. Engng Sci.* **25**, 1259–1266.

GROTBERG, J. B. & JENSEN, O. E. 2004 Biofluid mechanics in flexible tubes. *Ann. Rev. Fluid Mech.* **36**, 121–147.

HELFRICH, W. 1973 Elastic properties of lipid bilayers – theory and possible experiments. *Z. Naturforsch.* **28**, 693–703.

JENSEN, O. E., HORSBURGH, M. K., HALPERN, D. & GAVER, D. P. III 2002 The steady propagation of a bubble in a flexible-walled channel: asymptotic and computational models. *Phys. Fluids* **14**, 443–457.

KAOUI, B., RISTOW, G. H., CANTAT, I., MISBAH, C. & ZIMMERMANN, W. 2008 Lateral migration of a two-dimensional vesicle in unbounded poiseuille flow. *Phys. Rev.* E **77**, 021903.

KRECHETNIKOV, R. & HOMSY, G. M. 2005 Experimental study of substrate roughness and surfactant effects on the Landau–Levich law. *Phys. Fluids* **17**, 1021108.

KRUGLYAKOV, P. & NUSHTAYEVA, A. 2004 Emulsions stabilizied by solid particles: the role of capillary pressure in the emulsion films. In *Emulsions: Structure, Stability and Interactions* (ed. D. N. Petsev), Interface Science and Technology, vol. 4, pp. 641–676. Elsevier.

LANDAU, L. & LEVICH, B. 1942 Dragging of a liquid by a moving plate. *Acta Physicochim. USSR* **7**, 42–54.

MAYER, H. C. & KRECHETNIKOV, R. 2012 Landau–Levich flow visualization: revealing the flow topology responsible for the film thickening phenomena. *Phys. Fluids* **24**, 052103.

MCHALE, G. & NEWTON, M. I. 2011 Liquid marbles: principles and applications. *Soft Matt.* **7**, 5473–5481.

MCLEAN, J. W. & SAFFMAN, P. G. 1981 The effect of surface tension on the shape of fingers in a Hele Shaw cell. *J. Fluid Mech.* **102**, 455–469.

MONTEUX, C., KIRKWOOD, J., XU, H., JUNG, E. & FULLER, G. G. 2007 Determining the mechanical response of particle-laden fluid interfaces using surface pressure isotherms and bulk pressure measurements of droplets. *Phys. Chem. Phys.* **9**, 6344–6350.

NICOLSON, M. M. 1949 The interaction between floating particles. *Proc. Camb. Phil. Soc.* **45**, 288–295.

OKUBO, T. 1995 Surface tension of structured colloidal suspensions of polystyrene and silica spheres at air–water interface. *J. Colloid Interface Sci.* **171**, 55–62.

OURIEMI, M. & HOMSY, G. M. 2013 Experimental study of the effect of surface-adsorbed hydrophobic particles on the Landau–Levich law. *Phys. Fluids* (in press).

PARK, C.-W. 1991 Effects of insoluble surfactants on dip coating. *J. Colloid Interface Sci.* **146**, 382–394.

PARK, C.-W. & HOMSY, G. M. 1984 Two-phase displacement in Hele-Shaw cells: theory. *J. Fluid Mech.* **139**, 291–308.

PICKERING, S. U. 1907 Emulsions. *J. Chem. Soc. Trans.* **91**, 2001–2021.

PLANCHETTE, C., LORENCEAU, E. & BIANCE, A.-L. 2012 Surface wave on a particle raft. *Soft Matt.* **8**, 2444–2451.

POCIVAVSEK, L., DELLSY, R., KERN, A., JOHNSON, S., LIN, B., LEE, K. Y. C. & CERDA, E. 2008 Stress and fold localization in thin elastic membranes. *Science* **320**, 912–916.

PY, C., REVERDY, P., DOPPLER, L., BICO, JOSÉ, ROMAN, B. & BAROUD, C. N. 2007 Capillary origami: spontaneous wrapping of a droplet with an elastic sheet. *Phys. Rev. Lett.* **98**, 156103.

QUÉRÉ, D. 1999 Fluid coating on a fibre. *Ann. Rev. Fluid Mech.* **31**, 347–384.

RAMSDEN, W. 1903 Separation of solids in the surface-layers of solutions and 'suspensions' (Observations on surface-membranes, bubbles, emulsions and mechanical coagulation) – preliminary account. *Proc. R. Soc. Lond.* **72**, 156–164.

RATULOWSKI, J. & CHANG, H.-C. 1990 Marangoni effects of trace impurities on the motion of long gas bubbles in capillaries. *J. Fluid Mech.* **210**, 303–328.

REYNAERT, S., MOLDENAERS, P. & VERMANT, J. 2007 Interfacial rheology of stable and weakly aggregated two-dimensional suspensions. *Phys. Chem. Phys.* **9**, 6463–6475.

RIVETTI, M. & ANTKOWIAK, A. 2013 Elasto-capillary meniscus: pulling out a soft strip sticking to a liquid surface. *Preprint*.

SAFFMAN, P. G. & TAYLOR, G. I. 1958 The penetration of a fluid into a porous medum or Hele-Shaw cell containing a more viscous liquid. *Proc. R. Soc. Lond.* A **245**, 312–329.

SNOEIJER, J. H., ZIEGLER, J., ANDREOTTI, B., FERMIGIER, M. & EGGERS, J. 2008 Thick films of viscous fluid coating a plate withdrawn from a liquid reservoir. *Phys. Rev. Lett.* **100**, 244502.

STEBE, K. J. & BARTHÈS-BIESEL, D. 1995 Marangoni effects of adsorption–desorption controlled surfactants on the leading end of an infinitely long bubble in a capillary. *J. Fluid Mech.* **286**, 25–48.

SUBRAMANIAM, A. B., ABKARIAN, M., MAHADEVAN, L. & STONE, H. A. 2005*a* Non-spherical bubbles. *Nature* **438**, 938.

SUBRAMANIAM, A. B., ABKARIAN, M. & STONE, H. A. 2005*b* Controlled assembly of jammed colloidal shells on fluid droplets. *Nature Mater.* **4**, 553–556.

SZLEIFER, I., KRAMER, D., BEN-SHAUL, A., GELBART, W. M. & SAFRAN, S. A. 1990 Molecular theory of curvature elasticity in surfactant films. *J. Chem. Phys.* **92**, 6800–6817.

VAN DYKE, M. D. 1975 *Perturbation Methods in Fluid Mechanics*. Parabolic.

VANDEN-BROECK, J. M. 1984 Rising bubbles in a two-dimensional tube with surface tension. *Phys. Fluids* **27**, 2604–2607.

VARSHNEY, A., SANE, A., GHOSH, S. & BHATTACHARYA, S. 2012 Amorphous to amorphous transition in particle rafts. *Phys. Rev.* E **86**, 031402.

VELLA, D., AUSSILLOUS, P. & MAHADEVAN, L. 2004 Elasticity of an interfacial particle raft. *Europhys. Lett.* **68**, 212–218.

WÜRGER, A. 2000 Bending elasticity of surfactant films: the role of the hydrophobic tails. *Phys. Rev. Lett.* **85**, 337–340.

YUNKER, P. J., GRATALE, M., LOHR, M. A., STILL, T., LUBENSKY, T. C. & YODH, A. G. 2012 Influence of particle shape on bending rigidity of colloidal monolayer membranes and particle deposition during droplet evapouration in confined geometries. *Phys. Rev. Lett.* **108**, 228303.